

# Machine-learning invariant foliations in forced systems for reduced order modelling

Robert Szalai

20th March 2024

School of Engineering Mathematics and Technology, University of Bristol, Ada Lovelace Building, Tankard's Close, Bristol BS8 1TW, email: r.szalai@bristol.ac.uk

## Abstract

We identify reduced order models (ROM) of forced systems from data using invariant foliations. The forcing can be external, parametric, periodic or quasi-periodic. The process has four steps: 1. identify an approximate invariant torus and the linear dynamics about the torus; 2. identify a globally defined invariant foliation about the torus; 3. identify a local foliation about an invariant manifold that complements the global foliation 4. extract the invariant manifold as the leaf going through the torus and interpret the result. We combine steps 2 and 3, so that we can track the location of the invariant torus and scale the invariance equations appropriately. We highlight some fundamental limitations of invariant manifolds and foliations when fitting them to data, that require further mathematics to resolve.

## 1 Introduction

In this paper we develop a numerical method that identifies reduced order models (ROM) of deterministic and externally forced systems from data. A ROM is a self-contained system that tracks a small number of properties of the system over time accurately. Ideally, a ROM represents dynamics independent of the coordinate system in which the data is collected. This means that when a ROM is identified, a coordinate system, where the ROM is minimal, must also be identified [10]. There are many uses of a ROM, such as faster model predictions, identification of governing equations of physical phenomena and meaningful interpretation of data [8, 14].

In our definition, a genuine ROM discards unimportant dynamics [27], hence it does not reproduce the full data set. Instead, the ROM picks out a specific and simple phenomenon. A data set can yield many different ROMs, depending on what phenomenon we wish to extract. Only when all phenomena are identified can one reproduce the full data set. The coupling and relations among all identified ROMs can be recovered using the identified coordinate systems.

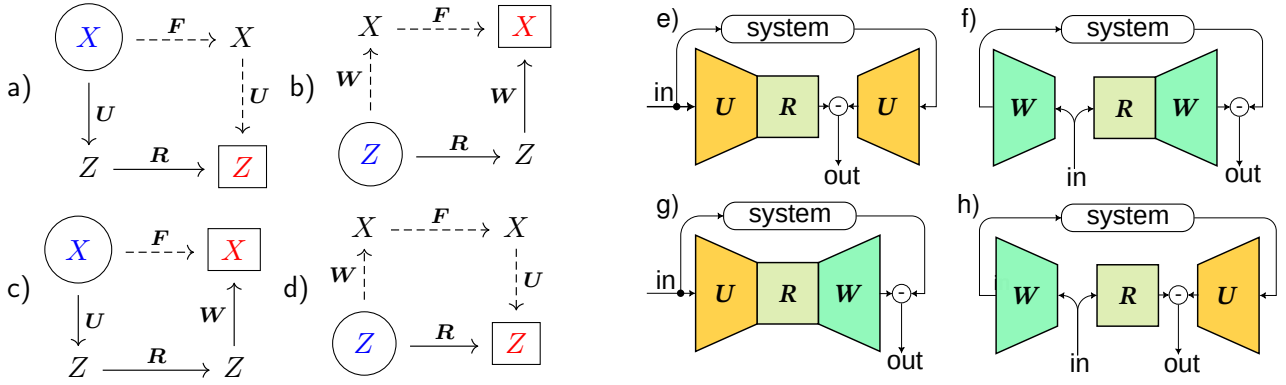


Figure 1: Commutative diagrams of a) invariant foliations, b) invariant manifolds, and connection diagrams of c) autoencoders and d) equation-free models. The dashed arrows denote the chain of function composition(s) that involves  $F$ , the continuous arrows denote the chain of function composition(s) that involves map  $R$ . The encircled vector space denotes the domain of the defining equation and the boxed vector space is the target of the defining equation. Diagrams (e,f,g,h) represent the defining equations corresponding to diagrams (a,b,c,d). The input (in) is the domain of the defining equation and the output (out) is the target, which must vanish.

The mathematical term for having a self-contained part of the system is *invariance*. Invariance means that the evolution of the system and the ROM are the same after a possibly non-invertible, but either surjective or injective transformation [27, Definition 1]. The transformation can either map from the physical coordinates to the state space of the ROM, which is called the encoder or in reverse, which is called the decoder. If we think of a system that maps an initial condition to a prediction, we need to relate the state of the system and the ROM to both the initial condition and the prediction. Given that we have a choice between an encoder and decoder for relating the ROM and the system, this gives us four architectures for ROM identification. The four possibilities are illustrated in figure 1 and are called invariant foliations [26], invariant manifolds [16], autoencoders [18] and equation-free models [17]. In what follows, we represent the encoder by function  $U$ , the decoder by  $W$ , the ROM by  $R$  and the (unknown) system by  $F$ . Often we cannot manipulate the initial conditions of our system, which precludes us from using a decoder when comparing initial conditions. This leaves us with invariant foliations and autoencoders to fit the data to. However, as discussed in [27], autoencoders cannot ensure invariance except when the dimensionality of the system and the dimensionality of the ROM are the same. Hence, only invariant foliations remain a possibility, which we use subsequently.

Invariant foliations are not a new idea [3, 22, 19], they are used to analyse chaotic systems [30]. Most similar to our application is, where an invariant foliation was used to find initial conditions for ROMs [23]. Elsewhere, invariant foliations are also called fibre bundles [1]. For data-driven reduced order modelling about fixed points, non-resonant invariant foliations were introduced in [26, 27], and their existence, uniqueness was proven using the parametrisation method [12, 15]. The geometric interpretation of an invariant foliation is explained in [19, 26].

In many circumstances it is necessary to identify an invariant manifold, represented by a decoder, that maps trajectories of the ROM back to the physical space, where that data came from. An invariant manifold can be calculated as a level set of an encoder of an invariant foliation that contains the equilibrium or (quasi-) periodic orbit. Therefore, we identify two invariant foliations from our data: one that captures the dynamics of interest and one that complements it. The accuracy of the second foliation is only important near the invariant manifold, which allows us to use a low-order (possibly linear) model that maps the leaves into each other. Having two complementary foliations also allows us to recover the equilibrium or (quasi-) periodic orbit, which lies at the intersection of the zero level sets of the two encoders.

The invariant foliation that captures the slowest dynamics is within the class of once differentiable foliations, which allows for an accurate ROM identification. However, the complementary foliation – and consequently the invariant manifold it defines – is only unique among foliations that are many times differentiable, depending on the spectral properties of the system. Moreover, the numerical error of calculating the invariant manifold scales with the power of the required order of differentiability for uniqueness. To

make this point precise let us consider the linear system

$$\begin{aligned}\dot{x} &= -x \\ \dot{y} &= -\frac{11}{2}y\end{aligned}$$

with trajectories  $y(x) = cx^{11/2}$ , where  $c$  is an integration constant. All trajectories are invariant manifolds, but the only smooth one is  $y(x) = 0$ . If we make a small numerical error of  $10^{-11}$  near the equilibrium, such that  $y(10^{-2}) = 10^{-11}$ , the error will be on the trajectory with  $c = 1$ , which gives an error at unit distance from the equilibrium of  $y(1) = 1$ . The error is not due to lack of invariance, because the result is an exact solution, instead we have chosen a manifold that is only five times differentiable as opposed to the required six. We used the fractional coefficient  $\frac{11}{2}$  to avoid talking about resonances.

As opposed to methods that carry out an asymptotic expansion of an invariant manifold about an invariant torus or equilibrium, we fit the foliation to data points and therefore the invariance equation is satisfied approximately at each data point. This can result in great differences from an asymptotically calculated invariant manifold, the resulting ROM is still accurate as it satisfies the invariance equation, sometimes better than the asymptotic expansion.

We note that there are other ways to single out a unique invariant manifold than smoothness, for example by exponential dichotomy [13]. The two definitions do not always coincide [12]. However, both approaches are local to the equilibrium or invariant torus, as opposed to data fitting, which is global. Data fitting cannot take smoothness or exponential dichotomy into account, because data points are discrete and we cannot differentiate over them. It is also unclear what a global minimum of a loss function represents and how it relates to asymptotic uniqueness criteria. It remains to be seen whether a global criterion that defines unique and meaningful invariant manifolds or foliations is possible.

The present paper is limited to a single set of parameters and therefore not suitable for bifurcation analysis. A trivial, parameter dependent extension, designates the parameters as state variables without any dynamics and adds some constraints to the numerical representation of the foliation.

The paper has three major sections. Section 2 summarises the relevant theory, section 3 introduces the numerical methods and section 4 illustrates the method on a number of example. The impatient reader can skip to section 3.

## 2 Set-up and invariant foliations

We assume a deterministic system and that the state of the system is sampled uniformly in time, giving us a series of data points. One part of the state is a real,  $n$ -dimensional inner product vector space  $X$ . The other part of the state is the  $d$ -dimensional torus  $\mathbb{T}^d$ , where the forcing occurs due to a rigid rotation  $\omega \in \mathbb{T}^d$ . The evolution of the state is described by a real analytic function  $\mathbf{F} : \mathbb{T}^d \times X$ , such that

$$\begin{aligned}\mathbf{x}_{k+1} &= \mathbf{F}(\mathbf{x}_k, \boldsymbol{\theta}_k) \\ \boldsymbol{\theta}_{k+1} &= \boldsymbol{\theta}_k + \omega\end{aligned}, \quad k = 1, 2, \dots \quad (1)$$

An invariant foliation is always specific to an underlying invariant object, which in our case is an invariant torus. The invariant torus can be parameterised over the torus  $\mathbb{T}^d$ , which we denote by

$$\mathcal{T} = \left\{ \mathbf{K}(\boldsymbol{\theta}) : \boldsymbol{\theta} \in \mathbb{T}^d \right\}, \quad (2)$$

where  $\mathbf{K} : \mathbb{T}^d \rightarrow X$  is an analytic function. The torus  $\mathcal{T}$  is invariant if the invariance equation

$$\mathbf{K}(\boldsymbol{\theta} + \omega) = \mathbf{F}(\boldsymbol{\theta}, \mathbf{K}(\boldsymbol{\theta})) \quad (3)$$

holds. Our numerical implementation uses  $d = 1$ , in which case the torus is a closed curve.

## 2.1 Linear dynamics

The calculation of invariant foliations depends on the linear dynamics about the invariant torus. Let us define

$$\mathbf{A}(\boldsymbol{\theta}) = D_1 \mathbf{F}(\mathbf{K}(\boldsymbol{\theta}), \boldsymbol{\theta})$$

and consider the linearised system

$$\begin{aligned} \mathbf{x}_{k+1} &= \mathbf{A}(\boldsymbol{\theta}_k) \mathbf{x}_k, \\ \boldsymbol{\theta}_{k+1} &= \boldsymbol{\theta}_k + \boldsymbol{\omega} \end{aligned}, \quad k = 1, 2, \dots \quad (4)$$

Instead of eigenvectors and eigenvalues, we need to use invariant vector bundles to decompose the dynamics of the linear system 4. Invariant foliations require the use of left vector bundles that satisfy the linear invariance equation

$$\boldsymbol{\Lambda}_j(\boldsymbol{\theta}) \mathbf{U}_j(\boldsymbol{\theta}) = \mathbf{U}_j(\boldsymbol{\theta} + \boldsymbol{\omega}) \mathbf{A}(\boldsymbol{\theta}), \quad (5)$$

where  $\mathbf{U}_j : \mathbb{T}^d \rightarrow \mathcal{L}(X, Z_j)$  and  $\boldsymbol{\Lambda}_j : \mathbb{T}^d \rightarrow \mathcal{L}(Z_j, Z_j)$  are analytic matrix valued functions and  $Z_j$  are a low-dimensional vector spaces. A complete decomposition means that  $X$  is isomorphic to  $\bigotimes_{j=1}^m Z_j$ , and  $\bigoplus_{j=1}^m (\ker \mathbf{U}_j(\boldsymbol{\theta}))^\perp = X$  for all  $\boldsymbol{\theta} \in \mathbb{T}^d$ . To characterise the linear dynamics, we use exponential dichotomies. The matrix  $\boldsymbol{\Lambda}_j$  has an exponential dichotomy for  $\rho \in \mathbb{R}^+$  if there exists  $C > 0$  such that the inequalities

$$\begin{aligned} |\boldsymbol{\Lambda}_j(\boldsymbol{\theta} + (k-1)\boldsymbol{\omega}) \cdots \boldsymbol{\Lambda}_j(\boldsymbol{\theta} + \boldsymbol{\omega}) \boldsymbol{\Lambda}_j(\boldsymbol{\theta})| &\leq C \rho^k, & \text{and} \\ \left| \boldsymbol{\Lambda}_j^{-1}(\boldsymbol{\theta} - k\boldsymbol{\omega}) \cdots \boldsymbol{\Lambda}_j^{-1}(\boldsymbol{\theta} - \boldsymbol{\omega}) \right| &\leq C \rho^{-k}, & \forall k \in \mathbb{N} \end{aligned}$$

hold. Our spectral decomposition is such that  $\boldsymbol{\Lambda}_j$  do not have exponential dichotomy when  $\rho \in \Sigma_j = [\alpha_j, \beta_j]$  but does anywhere else in  $\mathbb{R}^+$ . The sets  $\Sigma_j = [\alpha_j, \beta_j]$  are called spectral intervals, that are pairwise disjoint, i.e.  $\Sigma_j \cap \Sigma_k = \emptyset$  for  $j \neq k$ . We denote the number of spectral intervals by  $m$ .

For a constant matrix  $\mathbf{A}$ , the spectral intervals reduce to points ( $\alpha_j = \beta_j$ ), which are the magnitudes of the eigenvalues of  $\mathbf{A}$ . In addition, the row vectors of  $\mathbf{U}_j$  span the same space as the left eigenvectors of  $\mathbf{A}$  corresponding to the eigenvalues that have the magnitude  $\alpha_j = \beta_j$ . In section 3.3 we detail how to find  $\boldsymbol{\Lambda}_j$  and  $\mathbf{U}_j$  numerically by discretising (5) and turning it into an eigenvalue problem.

## 2.2 Invariant foliation

An invariant foliation is the solution of the invariance equation

$$\mathbf{R}(\mathbf{U}(\mathbf{x}, \boldsymbol{\theta}), \boldsymbol{\theta}) = \mathbf{U}(\mathbf{F}(\mathbf{x}, \boldsymbol{\theta}), \boldsymbol{\theta} + \boldsymbol{\omega}), \quad (6)$$

which also corresponds to the commutative diagram in figure 1(a). The functions  $\mathbf{R} : Z \times \mathbb{T}^d \rightarrow Z$  and  $\mathbf{U} : X \times \mathbb{T}^d \rightarrow Z$  in (6) are real analytic. In order to identify our foliation of interest, we select a number of spectral intervals using the index set

$$\mathcal{I} = \{i_1, i_2, \dots, i_{\#\mathcal{I}}\} \quad (7)$$

and stipulate that

$$D\mathbf{R}(\mathbf{0}, \boldsymbol{\theta}) = \begin{pmatrix} \boldsymbol{\Lambda}_{i_1}(\boldsymbol{\theta}) & & \mathbf{0} \\ & \ddots & \\ \mathbf{0} & & \boldsymbol{\Lambda}_{i_{\#\mathcal{I}}}(\boldsymbol{\theta}) \end{pmatrix} \text{ and } D\mathbf{U}(\mathbf{K}(\boldsymbol{\theta}), \boldsymbol{\theta}) = \begin{pmatrix} \mathbf{U}_{i_1}(\boldsymbol{\theta}) \\ \vdots \\ \mathbf{U}_{i_{\#\mathcal{I}}}(\boldsymbol{\theta}) \end{pmatrix}. \quad (8)$$

This means that the vector space of the conjugate dynamics  $\mathbf{R}$  is  $Z = \bigotimes_{j \in \mathcal{I}} Z_j$ . We also make the normalising assumption that  $\mathbf{U}(\mathbf{K}(\boldsymbol{\theta}), \boldsymbol{\theta}) = \mathbf{0}$ , from which it follows that  $\mathbf{R}(\mathbf{0}, \boldsymbol{\theta}) = \mathbf{0}$ . In what follows, we concurrently calculate the complementary foliation for index set  $\mathcal{I}^c = \{1, \dots, m\} \setminus \mathcal{I}$  using the invariance equation

$$\mathbf{S}(\mathbf{V}(\mathbf{x}, \boldsymbol{\theta}), \boldsymbol{\theta}) = \mathbf{V}(\mathbf{F}(\mathbf{x}, \boldsymbol{\theta}), \boldsymbol{\theta} + \boldsymbol{\omega}) \quad (9)$$

with similar boundary conditions except that  $\mathcal{I}$  is replaced by  $\mathcal{I}^c$ . We also define the vector space  $Z^c = \bigotimes_{j \in \mathcal{I}^c} Z_j$  and therefore the functions in equation (9) are  $\mathcal{S} : Z^c \times \mathbb{T}^d \rightarrow Z^c$  and  $\mathcal{V} : X \times \mathbb{T}^d \rightarrow Z^c$ .

The functions  $\mathbf{U}$  and  $\mathbf{R}$  are not unique, even when the foliation itself is unique. This is because any invertible transformation  $\mathbf{T} : Z \times \mathbb{T}^d \rightarrow Z$  can create a new encoder  $\tilde{\mathbf{U}}(\mathbf{x}, \boldsymbol{\theta}) = \mathbf{T}(\mathbf{U}(\mathbf{x}, \boldsymbol{\theta}), \boldsymbol{\theta})$  and conjugate map  $\tilde{\mathbf{R}}(\mathbf{z}, \boldsymbol{\theta}) = \mathbf{T}(\mathbf{R}(\mathbf{T}^{-1}(\mathbf{x}, \boldsymbol{\theta}), \boldsymbol{\theta}), \boldsymbol{\theta} + \boldsymbol{\omega})$ , which satisfy the invariance equation (6). A simple restriction to make the solution of (6) unique requires that

$$\mathbf{U}(\mathbf{W}(\boldsymbol{\theta})\mathbf{z}) = \mathbf{z}, \quad (10)$$

where  $\mathbf{W}$  satisfies the invariance equation

$$\mathbf{A}(\boldsymbol{\theta})\mathbf{W}(\boldsymbol{\theta}) = \mathbf{W}(\boldsymbol{\theta} + \boldsymbol{\omega})\mathbf{D}\mathbf{R}(\mathbf{0}, \boldsymbol{\theta}) \quad (11)$$

or just simply  $\mathbf{W}(\boldsymbol{\theta})\mathbf{D}\mathbf{V}(\mathbf{K}(\boldsymbol{\theta}), \boldsymbol{\theta}) = \mathbf{0}$ . It is not necessary that  $\mathbf{W}$  is accurately calculated, as the only requirement is that  $\mathbf{W}(\boldsymbol{\theta})\mathbf{D}\mathbf{U}(\mathbf{K}(\boldsymbol{\theta}), \boldsymbol{\theta})$  is invertible for all  $\boldsymbol{\theta} \in \mathbb{T}^d$ . In what follows, we will only restrict the nonlinear part of  $\mathbf{U}$ , so that  $U_{nl}(\mathbf{W}(\boldsymbol{\theta})\mathbf{z}) = \mathbf{0}$  for an approximate  $\mathbf{W}$ . Using  $\mathbf{W}$  that satisfies (11) leads to a so-called graph-style parametrisation akin to how invariant manifolds are parametrised in [7, Theorem 1.2].

*Remark 1.* It is important to think about the required value for parameter  $d$ , because an unnecessarily large number increases computational costs. A periodically forced system needs a single angle variable if the forcing frequency is not an integer multiple of the sampling frequency. However if the forcing frequency is an integer multiple of the sampling frequency, there is no need for an angle variable at all. Similarly, when there are multiple rationally unrelated forcing frequencies and one of the forcing frequencies is an integer multiple of the sampling frequency, we can use one less angle variables than the number of forcing frequencies. In reality, it might not be possible or desirable to synchronise forcing and sampling. In order to reproduce finer details of the signal and resolve higher harmonics, the sampling frequency cannot be a fraction of the forcing frequency, it must be at least twice as high as the lowest resolved frequency component, according to the Shannon-Nyquist theorem [24]. In these cases  $d$  must equal the number of rationally unrelated forcing frequencies. The case of a single forcing frequency is however special, because regardless of sampling, Floquet theory [11] applies to the underlying continuous-time system. This means that a time-dependent coordinate transformation can eliminate the angle variable from the linear part of (1) about the a periodic orbit. Making the nonlinear terms autonomous requires non-resonance conditions that we outline later.

A foliation might not exist if there are resonances among the spectral intervals. Even though we have assumed an analytic system, an invariant foliation can be finitely many times differentiable or only continuous. The theorem below states that among all possible foliations there is always an analytic one, which is unique.

**Theorem 2.** *Assume an invariant torus (2) and a linearised system about the torus in the form of (4). Also assume that the linear system has dichotomy spectral intervals  $\Sigma_j = [\alpha_j, \beta_j]$ ,  $1 \leq j \leq m$  and that  $\max \beta_j < 1$ . Pick one or more spectral intervals using a non-empty index set*

$$\mathcal{I} \subset \{1, 2, \dots, m\}$$

*with the condition that  $\alpha_j \neq 0$  for all  $j \in \mathcal{I}$  so that linear system (4) restricted to the subset of the spectrum*

$$\Sigma_{\mathcal{F}} = \bigcup_{j \in \mathcal{I}} \Sigma_j$$

*is invertible. Define the spectral quotient as*

$$\beth_{\mathcal{I}} = \frac{\min_{j \in \mathcal{I}} \log \alpha_j}{\log \beta_m}.$$

*If the non-resonance conditions*

$$1 \notin [\beta_{i_0}^{-1} \alpha_{i_1} \cdots \alpha_{i_j}, \alpha_{i_0}^{-1} \beta_{i_1} \cdots \beta_{i_j}] \quad (12)$$

*hold for  $i_0 \in \mathcal{I}$ ,  $i_1, \dots, i_j \in \{1, 2, \dots, m\}$  and  $2 \leq j < \beth_{\mathcal{I}} + 1$  with some  $i_k \notin \mathcal{I}$  then*

1. there exists a unique invariant foliation defined by analytic functions  $U$  and  $R$  satisfying equation (6) in a sufficiently small neighbourhood of the torus  $\mathcal{T}$  such that equations (8) hold;
2. the nonlinear map  $R$  is a polynomial, which in its simplest form contains terms for which the internal non-resonance conditions (12) with  $i_0, i_1, \dots, i_j \in \mathcal{I}$  and  $2 \leq j < \beth_{\mathcal{I}} + 1$  does not hold.

*Proof.* The details can be found in the paper [28]. □

### 3 The data and identifying the foliation

This section describes the numerical methods that lead to the identification and analysis of our ROM. To simplify the numerical method, we assume a one-dimensional torus. It is possible to use more frequencies at the expense of higher computational costs. The data we consider come in triplets  $\mathbf{x}^k, \mathbf{y}^k, \theta^k$ , such that

$$\mathbf{y}^k = \mathbf{F}(\mathbf{x}^k, \theta^k) + \boldsymbol{\xi}^k, \quad k = 1 \dots N, \quad (13)$$

where  $\boldsymbol{\xi}^k$  is a small perturbation drawn from a probability distribution with zero mean. Equation (13) is the unknown part of the dynamics, i.e., map  $\mathbf{F}$  is unknown. We assume that the external forcing is known, which is the second line of equation (1) with a fixed  $\omega \in \mathbb{T}$ . When considering trajectories for some set of consecutive indices we have  $\mathbf{x}^{k+1} = \mathbf{y}^k$  and  $\theta^{k+1} = \theta^k + \omega$ .

The notation we use from now on for matrix multiplications and tensor contractions is the following. A matrix multiplication  $\mathbf{C} = \mathbf{A}\mathbf{B}$  is denoted by  $C_{il} = A_{ij}B_{jl}$ . So whenever an index appears more than once on one side of an equation it is summed over. When we do not want to sum over an index, even if it appears in multiple factors, we underline the specific index, for example  $C_{ilk} = A_{ij\underline{k}}B_{jl\underline{k}}$ . The index notation implicitly assumes the existence of an orthonormal basis, for example a vector can be written as  $\mathbf{x} = x_i \mathbf{e}_i \in X$ , where  $\mathbf{e}_i \in X$ ,  $i \in \{1, \dots, n\}$  is a set of orthonormal basis vectors. Orthonormality allows us to use the same vectors for the dual basis, which greatly simplifies our notation.

#### 3.1 Discretisation and shift along the torus

We use Fourier collocation [29] to resolve functions on the torus  $\mathbb{T}$ . Fourier collocation demands a uniform grid, which is given by the nodes

$$\vartheta_1 = 0, \dots, \vartheta_{2\ell+1} = \frac{2\ell}{2\ell+1}2\pi, \quad (14)$$

where  $\ell$  is the number of harmonics to be resolved. A frequency limited function  $\mathbf{x} : \mathbb{T} \rightarrow \mathbb{R}^n$  can be reconstructed using

$$\mathbf{x}(\theta) = \sum_{j=1}^{2\ell+1} \gamma(\theta - \vartheta_j) \mathbf{x}_j,$$

where  $\mathbf{x}_j = \mathbf{x}(\vartheta_j)$  and

$$\gamma(\theta) = \frac{1}{2\ell+1} \frac{\sin \frac{2\ell+1}{2}\theta}{\sin \frac{1}{2}\theta}.$$

A function can also be represented by a two-index array  $x_{ij} = x_i(\vartheta_j)$ , where  $i$  is the coordinate index of  $\mathbf{x}$  in our basis  $\mathbf{e}_i$ . Interpolating a function at data points  $\theta^k$  can be written as  $x_i(\theta^k) = x_{ij}t_j^k$ , where  $t_j^k = \gamma(\theta^k - \vartheta_j)$ . Similarly, interpolating a matrix-valued function  $\mathbf{A} : \mathbb{T} \rightarrow \mathbb{R}^{n \times n}$  at the grid points can be written as  $A_{ij}(\theta^k) = A_{ijl}t_l^k$ .

A common operation with forced discrete-time systems is to shift a signal to the right by the angle  $\omega$ . The shift operator  $\mathcal{S}^\omega$  is defined as

$$(\mathcal{S}^\omega \mathbf{x})(\theta) = \mathbf{x}(\theta - \omega).$$

The discrete version of the shift operator is calculated from

$$\mathbf{y}_i = (\mathcal{S}^\omega \mathbf{x})(\vartheta_i) = \sum_{j=1}^{2\ell+1} \gamma(\vartheta_i - \vartheta_j - \omega) \mathbf{x}_j.$$

We then introduce the notation

$$\mathbb{S}_{jk}^\omega = \gamma(\vartheta_k - \vartheta_j - \omega),$$

so that a shifted representation of a function becomes  $y_{il} = x_{ij} \mathbb{S}_{jl}^\omega$ . Note that  $(\mathbb{S}^\omega)^T = \mathbb{S}^{-\omega}$ , because function  $\gamma$  is even.

### 3.2 Approximate invariant torus and nearby linear dynamics

In order to find the torus and the linear dynamics about the torus, we assume the following model

$$\mathbf{F}(\mathbf{x}, \theta) = \mathbf{A}(\theta) \mathbf{x} + \mathbf{b}(\theta),$$

where

$$\mathbf{A}(\theta) = \sum_{k=1}^{2\ell+1} \gamma(\theta - \vartheta_k) \mathbf{A}_k.$$

The linear model identification is iterative: we first use all data points and then remove data that is far from the initial guess of the torus to refine both the torus and the linear model near the torus. We also use scaling so that data points closer to the torus bear greater importance than data further from the torus. The initial model parameters are found by solving the optimisation problem

$$\arg \min_{\mathbf{A}, \mathbf{b}} \frac{1}{2} \sum_{k=1}^N \left\| \mathbf{A}(\theta^k) \mathbf{x}^k + \mathbf{b}(\theta^k) - \mathbf{y}^k \right\|^2. \quad (15)$$

After a solution to (15) we remove some of the data that are not close to the torus in Euclidean norm (the particular amount is problem dependent). The value of the norm in (15) vanishes on the invariant torus and therefore the fitting error near the torus would be assigned less importance without scaling. In order to make the significance of the relative fitting error approximately uniform over the data we introduce a scaling factor for each data point

$$\delta^k = \frac{1}{\epsilon^2 + \|\mathbf{x}^k - \mathbf{K}(\theta^k)\|^2}, \quad (16)$$

where  $\epsilon > 0$  is a small number, which we choose to be  $\epsilon = 2^{-8}$ . Factors  $\delta^k$  are updated after each iteration, otherwise they are considered constants. We apply the scaling factor  $\delta^k$  to each term in (15) and re-write it using our index notation into

$$\arg \min_{\mathbf{A}, \mathbf{b}} \frac{1}{2} \sum_{k=1}^N \delta^k \left\| A_{ijl} x_j^k t_l^k + b_{il} t_l^k - y_i^k \right\|^2, \quad (17)$$

which is a linear regression problem and can be solved directly. To elaborate this point, we define  $\tilde{A}_{ijl} = A_{ijl}$ ,  $\tilde{A}_{i(n+1)l} = b_{il}$  and  $\tilde{x}_{jl}^k = x_j^k t_l^k$ ,  $\tilde{x}_{(n+1)l}^k = t_l^k$  so that the loss function becomes

$$\arg \min_{\mathbf{A}, \mathbf{b}} \frac{1}{2} \sum_{k=1}^N \delta^k \left| \tilde{A}_{ijl} \tilde{x}_{jl}^k - y_i^k \right|^2,$$

which is a standard least squares problem [5] and has the solution of

$$\tilde{\mathbf{A}} = \mathbf{Y} \mathbf{X}^{-1},$$

where

$$X_{ijpq} = N^{-1} \sum_{k=1}^N \delta^k \tilde{x}_{ij}^k \tilde{x}_{pq}^k,$$

$$Y_{ipq} = N^{-1} \sum_{k=1}^N \delta^k y_i^k \tilde{x}_{pq}^k.$$

The iteration stops when the update to  $\tilde{\mathbf{A}}$  is smaller than machine precision.

The torus represented by function  $\mathbf{K}$  is calculated from the invariance equation

$$\mathbf{K}(\theta + \omega) = \mathbf{A}(\theta) \mathbf{K}(\theta) + \mathbf{b}(\theta)$$

that can be written using index notation as

$$K_{ij} \mathbb{S}_{jl}^{-\omega} = A_{ipl} K_{pl} + b_{il}. \quad (18)$$

Equation (18) is a Sylvester equation [2] and can be further transformed into the matrix-vector equation

$$(\delta_{ip} \mathbb{S}_{lq}^{\omega} - A_{ipq}) K_{pq} = b_{il}$$

that is solved using standard techniques for  $\mathbf{K}$  that represents the invariant torus.

### 3.3 Invariant vector bundles about the torus

We now want to solve the invariance equation (5) on the grid (14), which can be done by calculating the eigenvalues and eigenvectors of a discretised variant of (5). Such calculation assumes that  $\Lambda_j$  is constant. Note that we can only assume a constant  $\Lambda_j$ , when system (4) is reducible. It is however difficult to tell if a system is reducible numerically, so we will only observe the numerics breaking down. When fitting the invariant foliation to data, we mitigate problems arising from near irreducibility by normalising the calculated vector invariant bundle, that eventually makes  $\Lambda_j$  non-autonomous.

The discretised version of (5) is written as

$$\lambda \mathbf{u}^T(\vartheta_j) = \mathbf{u}^T(\vartheta_j + \omega) \mathbf{A}(\vartheta_j), \quad (19)$$

which translates to the eigenvector-eigenvalue problem

$$\left( \lambda \delta_{il} \delta_{jk} - \mathbb{S}_{jk}^{-\omega} A_{ilk} \right) u_{ij} = 0, \quad (20)$$

where  $\lambda$  is an eigenvalue and  $u_{ij}$  is an eigenvector. The eigenvalues are approximately placed along concentric circles in the complex plane and we expect that each circle contains an integer multiple of  $2\ell + 1$  eigenvalues. Using  $k$ -nearest neighbours [4], we attempt to find  $n_{cl} = n$  clusters for the magnitudes of the eigenvalues  $|\lambda|$ , expecting each cluster to have  $2\ell + 1$  eigenvalues. If such clusters cannot be found, we decrease  $n_{cl}$  until each cluster has an integer multiple of  $2\ell + 1$  eigenvalues while  $n_{cl} \geq n/2$ . It is possible to not find clusters that match our requirements, because of many reasons, for instance, the number of Fourier harmonics ( $\ell$ ) is too low, the actual spectral circles are too close to each other to resolve them numerically or there are multiplicities in the eigenvalues.

From each cluster, we choose the eigenvector that has the smallest dominant harmonic to form our vector bundle. Let us denote the eigenvalue and eigenvector pair of index  $p$  by  $\lambda_p$  and  $u_{ijp}$ , such that  $\mathbf{u}_p(\vartheta_j) = e_i u_{ijp}$ . The number of clusters is  $m$  and the set of indices that belong to cluster  $1 \leq k \leq m$  is  $cl(k)$ . The Fourier components of the eigenvectors are  $\tilde{u}_{ilp} = \sum_{j=1}^{2\ell+1} e^{-il\vartheta_j} u_{ijp}$ , where  $-\ell \leq l \leq \ell$ . In this notation, the index of the representative eigenvector and eigenvalue pair is calculated as

$$p_k = \arg \min_{p \in cl(k)} \left( \arg \max_l \sum_i |\tilde{u}_{ilp}|^2 \right). \quad (21)$$

If cluster  $k$  has only  $2\ell + 1$  eigenvalues, we expect that after multiplying the eigenvector with a scalar from the complex unit circle, it becomes a real-valued vector and we set

$$U_{1ij}^{d,k} = u_{ijp_k}, \quad \Lambda^k = \lambda_{p_k}. \quad (22)$$

If this is not the case, we reject the calculation. In the common case when cluster  $k$  contains  $2(2\ell + 1)$  eigenvalues, the real part and the imaginary part of the selected eigenvector represents the invariant bundle

$$U_{1ij}^{d,k} = \Re u_{ijp_k}, \quad U_{2ij}^{d,k} = \Im u_{ijp_k}, \quad \Lambda^k = \begin{pmatrix} \Re \lambda_{p_k} & -\Im \lambda_{p_k} \\ \Im \lambda_{p_k} & \Re \lambda_{p_k} \end{pmatrix}. \quad (23)$$



Given index set  $\mathcal{I}$ , defined by (7) and  $\mathcal{I}^c = \{1, \dots, m\} \setminus \mathcal{I} = \{j_1, \dots, j_{m-\#\mathcal{I}}\}$ , we set

$$\mathbf{U}^d = \begin{pmatrix} \mathbf{U}^{d,i_1} \\ \vdots \\ \mathbf{U}^{d,i_{\#\mathcal{I}}} \end{pmatrix}, \quad \mathbf{V}^d = \begin{pmatrix} \mathbf{U}^{d,j_0} \\ \vdots \\ \mathbf{U}^{d,j_{m-\#\mathcal{I}}} \end{pmatrix}, \quad (24)$$

and

$$\mathbf{R}^d = \begin{pmatrix} \boldsymbol{\Lambda}^{i_1} & & \mathbf{0} \\ & \ddots & \\ \mathbf{0} & & \boldsymbol{\Lambda}^{i_{\#\mathcal{I}}} \end{pmatrix}, \quad \mathbf{S}^d = \begin{pmatrix} \boldsymbol{\Lambda}^{j_1} & & \mathbf{0} \\ & \ddots & \\ \mathbf{0} & & \boldsymbol{\Lambda}^{j_{m-\#\mathcal{I}}} \end{pmatrix}.$$

For numerical reasons, we transform  $\mathbf{U}^d$ ,  $\mathbf{V}^d$ , so that at each grid point  $\vartheta_l$  they are orthogonal matrices. The transformation is carried out via singular value decomposition. We denote  $\mathbf{U}_l^d = \mathbf{U}^d(\vartheta_l)$  and its singular value decomposition by  $\mathbf{U}_l^d = \mathbf{G}_l^T \boldsymbol{\Sigma}_l \mathbf{H}_l$  and define  $\mathbf{U}_l^\square = \mathbf{G}_l^T \mathbf{H}_l$ . The transformation that brings back  $\mathbf{U}_l^\square$  into  $\mathbf{U}_l^d$  is  $\mathbf{T}_l = \mathbf{G}_l^T \boldsymbol{\Sigma}_l \mathbf{G}_l$ , such that  $\mathbf{U}_l^d = \mathbf{T}_l \mathbf{U}_l^\square$ . The linear invariance equation (5) now reads

$$\begin{aligned} \mathbf{R}^d \mathbf{T}(\theta) \mathbf{U}^\square(\theta) &= \mathbf{T}(\theta + \omega) \mathbf{U}^\square(\theta + \omega) \mathbf{A}(\theta) \\ \mathbf{T}^{-1}(\theta + \omega) \mathbf{R}^d \mathbf{T}(\theta) \mathbf{U}^\square(\theta) &= \mathbf{U}^\square(\theta + \omega) \mathbf{A}(\theta) \end{aligned}$$

and therefore  $\mathbf{U}^\square$  and

$$\mathbf{R}^\square(\theta) = \mathbf{T}^{-1}(\theta + \omega) \mathbf{R}^d \mathbf{T}(\theta) \quad (25)$$

also satisfy the invariance equation. Using index notation, the transformed linear map becomes  $R_{ijl}^\square = T_{ipr}^{-1} S_{rl}^{-\omega} R_{pq}^d T_{qjl}$ . We carry out the same transformation on  $\mathbf{V}^d$  and  $\mathbf{S}^d$ , to end up with a point-wise orthogonal  $\mathbf{V}^\square$  and  $\theta$ -dependent  $\mathbf{S}^\square$ .

In summary,  $\mathbf{U}^\square$  and  $\mathbf{V}^\square$  define a new coordinate system about the invariant torus in which the linear dynamics is block-diagonal, but not autonomous. In what follows, the data will be transformed into this coordinate systems, so that the functional representation of the identified invariant foliation is relatively simple.

### 3.4 Finding the invariant foliation

We now describe how to find the invariant foliation and a more accurate invariant torus relative to the approximate linear coordinate system calculated in section 3.3. Here we solve the invariance equations (6) and (9) together as they become coupled through scaling.

For numerical reasons, we transform our data into the time-dependent coordinate system calculated in section 3.3, which becomes

$$\begin{aligned} x_i^{k\parallel} &= U_{ijq}^\square t_q^k \left( x_j^k - K_{jl} t_l^k \right), & y_i^{k\parallel} &= U_{ijq}^\square t_q^k \left( y_j^k - K_{jl} S_{jp}^{-\omega} t_p^k \right), \\ x_i^{k\perp} &= V_{ijq}^\square t_q^k \left( x_j^k - K_{jl} t_l^k \right), & y_i^{k\perp} &= V_{ijq}^\square t_q^k \left( y_j^k - K_{jl} S_{jp}^{-\omega} t_p^k \right). \end{aligned} \quad (26)$$

The data points are accompanied by the interpolation weights on the torus, which are

$$t_j^k = \gamma \left( \theta^k - \vartheta_j \right), \quad t_j^{\omega k} = \gamma \left( \theta^k + \omega - \vartheta_j \right) = S_{jp}^{-\omega} t_p^k. \quad (27)$$

The numerical representation of the encoders present in the invariance equations (6) and (9) are given by

$$\begin{aligned} \mathbf{U}(\mathbf{x}^\parallel, \mathbf{x}^\perp, \theta) &= \mathbf{U}^c(\theta) + \mathbf{x}^\parallel + \mathbf{U}^l(\theta) \mathbf{x}^\perp + \mathbf{U}^{nl}(\mathbf{x}^\parallel, \mathbf{x}^\perp, \theta), \\ \mathbf{V}(\mathbf{x}^U, \mathbf{x}^V, \theta) &= \mathbf{V}^c(\theta) + \mathbf{x}^\perp + \mathbf{V}^l(\theta) \mathbf{x}^\parallel + \mathbf{V}^{nl}(\mathbf{x}^\parallel, \mathbf{x}^\perp, \theta), \end{aligned}$$

where

$$\begin{aligned} \mathbf{U}^c : \mathbb{T} &\rightarrow \mathbb{Z}, \quad \mathbf{U}^l : \mathbb{T} \rightarrow L(\mathbb{Z}^c, \mathbb{Z}), \quad \mathbf{U}^{nl} : \mathbb{Z} \times \mathbb{Z}^c \times \mathbb{T} \rightarrow \mathbb{Z}, \\ \mathbf{V}^c : \mathbb{T} &\rightarrow \mathbb{Z}^c, \quad \mathbf{V}^l : \mathbb{T} \rightarrow L(\mathbb{Z}, \mathbb{Z}^c), \quad \mathbf{V}^{nl} : \mathbb{Z} \times \mathbb{Z}^c \times \mathbb{T} \rightarrow \mathbb{Z}^c. \end{aligned}$$

To make the representation of any given pair of foliations unique, we normalise the encoders by applying the constraints

$$\mathbf{U}^{nl}(\mathbf{0}, \mathbf{x}^\perp, \theta) = \mathbf{0} \text{ and } \mathbf{V}^{nl}(\mathbf{x}^\parallel, \mathbf{0}, \theta) = \mathbf{0}, \quad (28)$$

which is the numerical equivalent of (10). The simplicity of the constraints (28) is a consequence of our coordinate transformation (26). As discussed in section 2.2, the constraints (28) need not be accurate, in fact there are many other valid constraints. However, the simplicity of (28) allows us to encode  $\mathbf{U}^{nl}$  and  $\mathbf{V}^{nl}$  in a straightforward manner. For example, if  $\mathbf{U}^{nl}$  is a polynomial, we drop all monomials that only contain components of  $\mathbf{x}^\perp$ . Let us denote  $\mathbf{x} = (\mathbf{x}^\parallel, \mathbf{x}^\perp)$ , then using a tensor product notation we have

$$\mathbf{U}^{nl}(\mathbf{x}^{k\parallel}, \mathbf{x}^{k\perp}, \theta^k) = \sum_{d=2}^{\sigma} \mathbf{U}_d^{nl} \mathbf{t}^k \otimes \mathbf{x}^\parallel \otimes \mathbf{x}^{\otimes d-1}, \quad (29)$$

which can represent any order- $\sigma$  polynomial that satisfy (28). The representation (29) can either use dense polynomials or polynomials with compressed tensor coefficients as described in [27].

For the conjugate dynamics represented by function  $\mathbf{R}$  in the invariance equations (6), we use a dense polynomial, because it is a low-dimensional function. For the conjugate dynamics of the complementary foliation  $\mathbf{S}$ , we either use a dense polynomial if we are dealing with a low-dimensional system, or a matrix in high dimensions. In fact, function  $\mathbf{S}$  can be linear if we consider a small neighbourhood of the invariant manifold defined by

$$\mathcal{M} = \left\{ (\mathbf{x}^\parallel, \mathbf{x}^\perp, \theta) \in X : \mathbf{V}(\mathbf{x}^\parallel, \mathbf{x}^\perp, \theta) = \mathbf{0} \right\}. \quad (30)$$

This is because in the neighbourhood of  $\mathcal{M}$ , the magnitude of  $\mathbf{V}$  is small. During the solution process of the invariance equation (9), the closer we get to the accurate solution, the data can be filtered, so that the value of  $\mathbf{V}$  over the remaining data set becomes small, as long as sufficient amount of data remains.

We define the relative error of the invariance equation by

$$E_{rel} = \frac{\|\mathbf{R}(\mathbf{U}(\mathbf{x}^\parallel, \mathbf{x}^\perp, \theta), \theta) - \mathbf{U}(\mathbf{y}^\parallel, \mathbf{y}^\perp, \theta + \omega)\|}{\|(\mathbf{x}^\parallel - \mathbf{K}^\parallel(\theta), \mathbf{x}^\perp - \mathbf{K}^\perp(\theta))\|}, \quad (31)$$

where  $\mathbf{K}^\parallel$  and  $\mathbf{K}^\perp$  represent the torus in the transformed coordinate system. The torus representation is the solution of

$$\mathbf{U}(\mathbf{K}^\parallel(\theta), \mathbf{K}^\perp(\theta), \theta) = \mathbf{0}, \quad \mathbf{V}(\mathbf{K}^\parallel(\theta), \mathbf{K}^\perp(\theta), \theta) = \mathbf{0}.$$

In order to make sure that the relative error is nearly uniform we scale the invariance equations (6) and (9) similar to how  $E_{rel}$  is calculated. Let us define

$$\delta^k = 1 + \frac{1}{\epsilon^2 + \|\mathbf{x}^{k\parallel} - \mathbf{K}^\parallel \mathbf{t}^k\|^2 + \|\mathbf{x}^{k\perp} - \mathbf{K}^\perp \mathbf{t}^k\|^2}$$

and use the loss function

$$L = \sum_{k=1}^N \delta^k \left( \|\mathbf{R} \circ \mathbf{U} - \mathbf{U}^\omega\|^2 + \|\mathbf{S} \circ \mathbf{V} - \mathbf{V}^\omega\|^2 \right). \quad (32)$$

where

$$\begin{aligned} \mathbf{U} &:= \mathbf{U}(\mathbf{x}^{k\parallel}, \mathbf{x}^{k\perp}, \mathbf{t}^k), & \mathbf{R} \circ \mathbf{U} &:= \mathbf{R}(\mathbf{U}(\mathbf{x}^{k\parallel}, \mathbf{x}^{k\perp}, \mathbf{t}^k), \mathbf{t}^k), & \mathbf{U}^\omega &:= \mathbf{U}(\mathbf{y}^{k\parallel}, \mathbf{y}^{k\perp}, \mathbf{t}^{\omega k}), \\ \mathbf{V} &:= \mathbf{V}(\mathbf{x}^{k\parallel}, \mathbf{x}^{k\perp}, \mathbf{t}^k), & \mathbf{S} \circ \mathbf{V} &:= \mathbf{S}(\mathbf{V}(\mathbf{x}^{k\parallel}, \mathbf{x}^{k\perp}, \mathbf{t}^k), \mathbf{t}^k), & \mathbf{V}^\omega &:= \mathbf{V}(\mathbf{y}^{k\parallel}, \mathbf{y}^{k\perp}, \mathbf{t}^{\omega k}) \end{aligned}$$

with data coming from (26) and (27). The initial values of the parameters are such that

$$\begin{aligned} \mathbf{R}(z, \theta) &= \mathbf{R}^1(\theta) z, \quad \mathbf{U}^c(\theta) = \mathbf{0}, \quad \mathbf{U}^l(\theta) = \mathbf{0}, \quad \mathbf{U}^{nl}(\mathbf{x}^\perp, \theta) = \mathbf{0}, \\ \mathbf{S}(z, \theta) &= \mathbf{S}^1(\theta) z, \quad \mathbf{V}^c(\theta) = \mathbf{0}, \quad \mathbf{V}^l(\theta) = \mathbf{0}, \quad \mathbf{V}^{nl}(\mathbf{x}^\perp, \theta) = \mathbf{0} \end{aligned}$$

with values from (25). The optimisation algorithm uses a batch coordinate descent technique [20], because in each individual component of the functional representation, the problem is nearly linear, while considering all parameters at the same time would be a more difficult problem. The scaling factors  $\delta^k$  and hence the invariant torus  $\mathbf{K}^\parallel$  and  $\mathbf{K}^\perp$  are updated after the optimisation step for a component has concluded. This same technique was used for autonomous systems in [27].

### 3.5 Recovering the invariant manifold

We now recover the invariant manifold from the two invariant foliations. The invariant manifold is defined by (30), which does not stipulate how it is parameterised. We however want the invariant manifold to have the same parametrisation as the invariant foliation defined by encoder  $\mathbf{U}$ , which means that the conjugate dynamics defined by  $\mathbf{R}$  will be the same for the invariant manifold. We now decompose the decoder of the invariant manifold into two components in  $X = Z \oplus Z^c$  and denote it by  $\mathbf{W}(z, \theta) = (\mathbf{W}^\parallel(z, \theta), \mathbf{W}^\perp(z, \theta))$ . The unknown decoder functions are found by solving the equations

$$\left. \begin{aligned} \mathbf{U}(\mathbf{W}^\parallel(z, \theta), \mathbf{W}^\perp(z, \theta), \theta) &= z \\ \mathbf{V}(\mathbf{W}^\parallel(z, \theta), \mathbf{W}^\perp(z, \theta), \theta) &= \mathbf{0} \end{aligned} \right\}. \quad (33)$$

Equations (33) can be re-written to the following form

$$\begin{pmatrix} \mathbf{I} & \mathbf{U}^l(\theta) \\ \mathbf{V}^l(\theta) & \mathbf{I} \end{pmatrix} \begin{pmatrix} \mathbf{W}^\parallel \\ \mathbf{W}^\perp \end{pmatrix} = \begin{pmatrix} z - \mathbf{U}^c(\theta) - \mathbf{U}^{nl}(\mathbf{W}^\perp, \theta) \\ \mathbf{0} - \mathbf{V}^c(\theta) - \mathbf{V}^{nl}(\mathbf{W}^\parallel, \theta) \end{pmatrix},$$

which can be solved by the iteration

$$\begin{pmatrix} \mathbf{W}^\parallel \\ \mathbf{W}^\perp \end{pmatrix} = \begin{pmatrix} \mathbf{I} & \mathbf{U}^l(\theta) \\ \mathbf{V}^l(\theta) & \mathbf{I} \end{pmatrix}^{-1} \begin{pmatrix} z - \mathbf{U}^c(\theta) - \mathbf{U}^{nl}(\mathbf{W}^\perp, \theta) \\ \mathbf{0} - \mathbf{V}^c(\theta) - \mathbf{V}^{nl}(\mathbf{W}^\parallel, \theta) \end{pmatrix}.$$

Given that our functions are represented by polynomials, the iteration will converge from the initial guess  $\mathbf{W}^\parallel = \mathbf{0}$ ,  $\mathbf{W}^\perp = \mathbf{0}$  to a polynomial of the same order as  $\mathbf{U}^{nl}$ ,  $\mathbf{V}^{nl}$  in the same number of steps as the highest polynomial order of  $\mathbf{U}^{nl}$ ,  $\mathbf{V}^{nl}$ .

### 3.6 Normal form transformation of the conjugate dynamics

In order to extract information from the conjugate dynamics  $\mathbf{R}$ , we transform it into its simplest form. This is the place where we account for internal and parametric resonances. The transformation uses the invariant manifold style to create a decoder. This style is useful when we have an invariant manifold, for example as a result of the recovery procedure in section 3.5.

The invariance equation we use is given by

$$\mathbf{T}(\check{\mathbf{R}}(z, \theta), \theta + \omega) - \mathbf{R}^d(\mathbf{T}(z), \theta) = \mathbf{0}, \quad (34)$$

where  $\mathbf{T} : Z \times \mathbb{T} \rightarrow Z$  is the transformation and  $\check{\mathbf{R}}$  is the normal form. The map  $\mathbf{R}^d$  with diagonalised linear part is calculated by

$$\mathbf{R}^d(z, \theta) = \mathbf{U}^d(\theta + \omega) \mathbf{R} \left( \left( \mathbf{U}^d(\theta) \right)^{-1} z, \theta \right),$$

where  $\mathbf{R}$  is the conjugate dynamics that we obtained from our invariant foliation also associated with the recovered invariant manifold  $\mathcal{M}$  in equation (30). The linear transformation  $\mathbf{U}^d$  is the full invariant bundle decomposition of  $D_1 \mathbf{R}(\mathbf{0}, \cdot)$  calculated using the methods discussed in section 3.3, and given by formula (24) for an index set  $\mathcal{I}$  that covers the full dichotomy spectrum of  $D_1 \mathbf{R}(\mathbf{0}, \cdot)$ . After the transformation, we have  $\mathbf{R}^d(z, \theta) = \mathbf{\Lambda}z + \mathbf{N}(z, \theta)$ , where  $\mathbf{\Lambda}$  is diagonal, with possibly complex entries and  $\mathbf{N}(z, \theta) = \mathcal{O}(|z|^2)$ .

We represent the solution of (34) by trigonometric power series

$$\left. \begin{aligned} \mathbf{T}(z, \theta) &= \sum_{j=1}^{\sigma} \mathbf{T}^j(\theta) z^{\otimes j} \\ \check{\mathbf{R}}(z, \theta) &= \sum_{j=1}^{\sigma} \check{\mathbf{R}}^j(\theta) z^{\otimes j} \end{aligned} \right\}, \quad (35)$$

where

$$\left. \begin{aligned} \mathbf{T}^j(\theta) z^{\otimes j} &= \sum_{i_0 \dots i_j, k} e_{i_0} T_{i_0 i_1 \dots i_j}^{j, k} e^{ik\theta} z_{i_1} \dots z_{i_j}, \\ \check{\mathbf{R}}^j(\theta) z^{\otimes j} &= \sum_{i_0 \dots i_j, k} e_{i_0} \check{R}_{i_0 i_1 \dots i_j}^{j, k} e^{ik\theta} z_{i_1} \dots z_{i_j}, \end{aligned} \right\} \quad (36)$$

and  $e_i$ ,  $i \in \{1, \dots, \dim Z\}$  is our orthonormal basis in  $Z$ . Substituting the ansatz (35) into (34) and separating the  $j$ th order terms leads to the homological equation

$$\mathbf{T}^1(\theta + \omega) \check{\mathbf{R}}^j(\theta) z^{\otimes j} + \mathbf{T}^j(\theta + \omega) (\Lambda x)^{\otimes j} - \Lambda \mathbf{T}^j(\theta) z^{\otimes j} = \Gamma^j(\theta) z^{\otimes j}, \quad (37)$$

where  $\Gamma^j(\theta)$  are terms composed of  $\mathbf{R}^d$  and  $\mathbf{T}$  of order lower than  $j$ . Successively solving equation (37) leads to a normal form.

For the linear terms, the solution of equation (37) can be chosen as  $\mathbf{T}^1(\theta) = \mathbf{I}$  and  $\check{\mathbf{R}}^1(\theta) = \Lambda$ . The nonlinear terms are determined from equation

$$\check{R}_{i_0 i_1 \dots i_j}^{j, k} + \lambda_{i_1} \dots \lambda_{i_j} e^{ik\omega} T_{i_0 i_1 \dots i_j}^{j, k} - \lambda_{i_0} T_{i_0 i_1 \dots i_j}^{j, k} = \Gamma_{i_0 i_1 \dots i_j}^{j, k},$$

which has the solution

$$T_{i_0 i_1 \dots i_j}^{j, k} = \frac{1}{\lambda_{i_1} \dots \lambda_{i_j} e^{ik\omega} - \lambda_{i_0}} \Gamma_{i_0 i_1 \dots i_j}^{j, k} \quad \check{R}_{i_0 i_1 \dots i_j}^{j, k} = 0 \text{ or} \quad (38)$$

$$T_{i_0 i_1 \dots i_j}^{j, k} = 0 \quad \check{R}_{i_0 i_1 \dots i_j}^{j, k} = \Gamma_{i_0 i_1 \dots i_j}^{j, k}. \quad (39)$$

We call the case when  $\lambda_{i_1} \dots \lambda_{i_j} e^{ik\omega} - \lambda_{i_0} \approx 0$  an internal resonance, in which case the solution (39) is used. As per our assumptions we only allow internal resonance for  $k = 0$ , which leads to an autonomous normal form.

Putting together all transformations, we define

$$\check{\mathbf{W}}(z, \theta) = \mathbf{W} \left( \left( \mathbf{U}^d(\theta) \right)^{-1} \mathbf{T}(z, \theta), \theta \right).$$

We find that the normal form  $\check{\mathbf{R}}$  satisfies the manifold invariance equation

$$\check{\mathbf{W}} \left( \check{\mathbf{R}}(z, \theta), \theta + \omega \right) = \check{\mathbf{F}} \left( \check{\mathbf{W}}(z, \theta), \theta \right),$$

where  $\check{\mathbf{F}}$  is the unknown system in the frame of the approximate vector bundles defined by  $\mathbf{U}^1$ ,  $\mathbf{V}^1$ .

### 3.7 Frequencies and damping ratios

We now assume that the normal form transformation in section 3.6 has led to an autonomous system, that is  $\check{\mathbf{R}}(z, \theta) = \check{\mathbf{R}}(z)$ . When we calculate the invariant foliation for a vector bundle associated with a complex conjugate pair of eigenvalues, the conjugate dynamics can also be written as a pair of complex conjugate functions [30] of the complex variable  $z$  in the form of

$$\check{\mathbf{R}}(z) = \begin{pmatrix} s(z, \bar{z}) \\ \bar{s}(z, \bar{z}) \end{pmatrix},$$

where  $\bar{\phantom{x}}$  means complex conjugate. We now define

$$\begin{aligned} \widehat{\mathbf{W}}(r, \beta, \theta) &= \check{\mathbf{W}} \left( re^{i\beta}, re^{-i\beta}, \theta \right), \\ R(r) &= \left| s \left( re^{i\beta}, re^{-i\beta} \right) \right| \\ T(r) &= \arg e^{-i\beta} s \left( re^{i\beta}, re^{-i\beta} \right) \end{aligned}$$

and the invariance equation becomes

$$\widehat{\mathbf{W}}(R(r), \beta + T(r), \theta + \omega) = \mathbf{F}\left(\widehat{\mathbf{W}}(r, \beta, \theta), \theta\right).$$

Functions  $R$  and  $T$  are independent of  $\beta$  because we have eliminated this dependence during the normal-form transformation by only keeping near resonant terms.

The functions  $R$  and  $T$  also relate to the damping and the frequency of the dynamics, in fact if we were to consider  $Z$  as an Euclidean frame, the frequency of the dynamics would be  $\omega(r) = T(r) / \Delta t$  and the damping would be  $\xi(r) = \log(r^{-1}R(r)) / T(r)$ . However the decoder  $\widehat{\mathbf{W}}$  defines a nonlinear frame in  $X$  and therefore we need to calculate the damping and the frequency by taking into account the nonlinearity of  $\widehat{\mathbf{W}}$ .

There are two factors that makes the calculations inaccurate: the amplitude predicted by  $\widehat{\mathbf{W}}$  does not increase linearly with parameter  $r$  and the phase angles of two  $d + 1$  dimensional tori for two fixed values of  $r$  do not align in  $X$  and therefore when a solution decays, in each cycle a phase shift occurs relative to what  $T(r)$  predicts, which leads to a frequency miscalculation. Here we fix both of these discrepancies.

To carry out the correction we use the transformation  $r = \rho(\hat{r})$  and  $\beta = \hat{\beta} + \alpha(\rho(\hat{r}))$ , where  $\rho : [0, \infty) \rightarrow [0, \infty)$  and  $\alpha : [0, \infty) \rightarrow \mathbb{R}$ , and define

$$\tilde{\mathbf{W}}(r, \beta, \theta) = \widehat{\mathbf{W}}(\rho(r), \beta + \alpha(\rho(r)), \theta). \quad (40)$$

This transformation re-scales the amplitude and introduces an amplitude dependent phase shift. We do not shift the phase of the forcing, because that would make the forcing frequency dependent on the vibration amplitude. The two-dimensional tori parametrised by the amplitude parameter are

$$\mathcal{T}_r = \left\{ \tilde{\mathbf{W}}(r, \beta, \theta) : \beta, \theta \in [0, 2\pi) \right\}.$$

To make sure that the amplitude of the torus grows linearly with  $r$ , we impose the constraint

$$(2\pi)^{-2} \int_{\mathbb{T}^2} \left| \widehat{\mathbf{W}}(\rho(r), \beta, \theta) \right|^2 d\beta d\theta = r^2. \quad (41)$$

We also impose zero phase shift between nearby tori  $\mathcal{T}_r$  and  $\mathcal{T}_{r+\epsilon}$  using the constraint

$$\arg \min_{\delta} \int_{\mathbb{T}^2} \left| \widehat{\mathbf{W}}(\rho(r+\epsilon), \beta + \alpha(\rho(r+\epsilon)) + \delta, \theta) - \widehat{\mathbf{W}}(\rho(r), \beta + \alpha(\rho(r)), \theta) \right|^2 d\beta d\theta \Big|_{\delta=0} = 0, \quad (42)$$

which stipulates that the distance between the points on the two tori corresponding at the same parameters is minimal on average at zero additional phase shift  $\delta = 0$ . To satisfy constraint (41), we define the function

$$\kappa(\rho) = (2\pi)^{-(d+1)/2} \sqrt{\int_{\mathbb{T}^2} \left| \widehat{\mathbf{W}}(\rho(r), \beta, \theta) \right|^2 d\beta d\theta},$$

and set

$$\rho(r) = \kappa^{-1}(r).$$

The necessary condition to find a minimum of (42) is a vanishing gradient, hence we calculate the gradient of

$$L(\delta) = \frac{1}{2} \int_{\mathbb{T}^2} \left| \widehat{\mathbf{W}}(\rho(r+\epsilon), \beta + \alpha(\rho(r+\epsilon)) + \delta, \theta) - \widehat{\mathbf{W}}(\rho(r), \beta + \alpha(\rho(r)), \theta) \right|^2 d\beta d\theta,$$

at  $\delta = 0$ , which leads to the equation of the necessary condition

$$\int_{\mathbb{T}^2} \left\langle \widehat{\mathbf{W}}(\rho(r+\epsilon), \beta + \alpha(\rho(r+\epsilon)), \theta) - \widehat{\mathbf{W}}(\rho(r), \beta + \alpha(\rho(r)), \theta), D_2 \widehat{\mathbf{W}}(\rho(r+\epsilon), \beta + \alpha(\rho(r+\epsilon)), \theta) \right\rangle d\beta d\theta = 0. \quad (43)$$

Dividing equation (43) by  $\epsilon$  and letting  $\epsilon \rightarrow 0$ , we obtain

$$\begin{aligned} \lim_{\epsilon \rightarrow 0} \epsilon^{-1} \left[ \widehat{\mathbf{W}}(\rho(r+\epsilon), \beta + \alpha(\rho(r+\epsilon)), \theta) - \widehat{\mathbf{W}}(\rho(r), \beta + \alpha(\rho(r)), \theta) \right] \\ = D_1 \widehat{\mathbf{W}}(\rho(r), \beta + \alpha(\rho(r)), \theta) \dot{\rho}(r) + D_2 \widehat{\mathbf{W}}(\rho(r), \beta + \alpha(\rho(r)), \theta) \dot{\alpha}(\rho(r)) \dot{\rho}(r) = 0. \end{aligned}$$

Further eliminating the non-zero  $\dot{\rho}$  and substituting  $r \rightarrow \rho^{-1}(r)$ , we get

$$\int_{\mathbb{T}^2} \left\langle D_1 \widehat{\mathbf{W}}(r, \beta, \theta) + D_2 \widehat{\mathbf{W}}(r, \beta, \theta) \dot{\alpha}(r), D_2 \widehat{\mathbf{W}}(r, \beta, \theta) \right\rangle d\beta d\theta = 0,$$

whose solution for  $\dot{\alpha}$  is

$$\dot{\alpha}(r) = - \left[ \int_{\mathbb{T}^2} \left\langle D_2 \widehat{\mathbf{W}}(r, \beta, \theta), D_2 \widehat{\mathbf{W}}(r, \beta, \theta) \right\rangle d\beta d\theta \right]^{-1} \int_{\mathbb{T}^2} \left\langle D_1 \widehat{\mathbf{W}}(r, \beta, \theta), D_2 \widehat{\mathbf{W}}(r, \beta, \theta) \right\rangle d\beta d\theta. \quad (44)$$

The expression of  $\dot{\alpha}$  can be integrated with initial condition  $\alpha(0) = 0$  to recover the required phase shift.

The new parametrisation as defined by equation (40) satisfies the invariance equation

$$\tilde{\mathbf{W}}(\tilde{R}(r), \beta + \tilde{T}(r), \theta) = \overline{\mathbf{F}}(\tilde{\mathbf{W}}(r, \beta, \theta), \theta),$$

where

$$\begin{aligned} \tilde{R}(r) &= \rho^{-1}(R(\rho(r))), \\ \tilde{T}(r) &= T(\rho(r)) + \alpha(\rho(r)) - \alpha(R(\rho(r))). \end{aligned}$$

Finally, the instantaneous frequency and damping ratio becomes

$$\begin{aligned} \omega(r) &= \tilde{T}(r) / \Delta t \\ \xi(r) &= \log(r^{-1} \tilde{R}(r)) / \tilde{T}(r), \end{aligned}$$

respectively, where  $\Delta t$  is the sampling period. The ROM with accurate frequencies and damping can be written in the ordinary differential equation form

$$\begin{aligned} \dot{r} &= -\zeta(r) \omega(r) r, \\ \dot{\theta} &= \omega(r). \end{aligned}$$

### 3.8 Summary of ROM identification

The ROM identification has generally three major steps, that can be characterised as pre-processing the data, fitting the foliation to data and analysing the result. Each major step can be broken down into smaller tasks as follows.

1. Pre-processing the data
  - (a) Identification of an approximate invariant torus and the linear dynamics about the torus. (Section 3.2.)
  - (b) Decomposition of the linear dynamics into invariant vector bundles. (Section 3.3.)
  - (c) Transforming the data into the coordinate system of the vector bundles. (Equations (26) and (27).)
2. Fitting two invariant foliations to the data, one that contains the dynamics of interest and one that is possibly less accurate, but defines the invariant manifold of the the dynamics of interest. (Section 3.4.)
3. Post-processing the result
  - (a) Recovering the invariant manifold from the foliation. (Section 3.5.)
  - (b) If necessary, calculate instantaneous frequencies and damping ratios that are accurate. (Sections 3.6 and 3.7.)

In what follows we illustrate this procedure through examples.

## 4 Examples

We will use synthetic data as the author does not have access to experimental data of the kind necessary to demonstrate the method. In addition to the methods discussed, we also calculate invariant manifolds directly from vector fields. This includes finding the invariant torus and calculating the invariant vector bundles about the torus [28]. We also use a facility in the Julia programming language that allows Taylor expansion of solutions of differential equations through automatic differentiation. Hence we can also calculate invariant manifolds and invariant foliations from the generated maps without using simulation data.

In what follows we will also display the eigenvalues (20) in a vector field form, that is

$$\lambda_{vf} = \frac{1}{\Delta t} \log \lambda_{map}$$

This helps visualisation, because eigenvalues are now appear on vertical lines as opposed to concentric circles. We analyse the relative error (31) of our calculations with respect to the invariance equation (6). To provide a basis for comparison we solve the manifold invariance equation for the underlying ordinary differential equation in our examples, which is

$$D_1 \mathbf{W}(\mathbf{z}, \theta) \mathbf{R}(\mathbf{z}, \theta) + \omega_0 D_2 \mathbf{W}(\mathbf{z}, \theta) = \mathbf{f}(\mathbf{W}(\mathbf{z}, \theta), \theta), \quad (45)$$

where  $\mathbf{f}$  represents the ordinary differential equation

$$\begin{aligned} \dot{\mathbf{x}} &= \mathbf{f}(\mathbf{x}, \theta), \\ \dot{\theta} &= \omega_0. \end{aligned}$$

The solution methods is similar to the normal for transformation detailed in section 3.6. For the direct calculation we use

$$E_{rel}(\mathbf{z}, \theta) = \frac{\|D_1 \mathbf{W}(\mathbf{z}, \theta) \mathbf{R}(\mathbf{z}, \theta) + \omega_0 D_2 \mathbf{W}(\mathbf{z}, \theta) - \mathbf{f}(\mathbf{W}(\mathbf{z}, \theta), \theta)\|}{\|\mathbf{W}(\mathbf{z}, \theta)\|} \quad (46)$$

for the relative error and  $\|\mathbf{W}(\mathbf{z}, \theta)\|$  for the amplitude.

### 4.1 Shaw-Pierre oscillator

We consider a variant of the well-studied example of reduced order modelling that appeared in [25]. The equations of motions are written as

$$\begin{aligned} \dot{x}_1 &= x_3, \\ \dot{x}_2 &= x_4, \\ \dot{x}_3 &= -cx_3 - kx_1 - \kappa y_1^3 + k(y_2 - y_1) + c(y_4 - y_3) + A \cos(\omega t + 0.1), \\ \dot{x}_4 &= -cy_4 - ky_2 - k(y_2 - y_1) - c(y_4 - y_3) + A \cos(\omega t). \end{aligned} \quad (47)$$

We choose the parameters  $k = 1$ ,  $\kappa = 0.2$  and  $c = 2^{-5}$ . The unforced natural frequencies are  $\omega_1 = 1$  and  $\omega_2 = 1.7314$  and the damping ratios are  $\zeta_1 = 0.0156$  and  $\zeta_2 = 0.0271$ . The spectral quotients are  $\beth_1 = 1$  and  $\beth_2 = 3$ . When we turn on the forcing at  $A = 0.25$ , the frequencies become  $\omega_1 = 1.0263$ ,  $\omega_2 = 1.7473$ , the damping ratios become  $\zeta_1 = 0.0153$ ,  $\zeta_2 = 0.0268$ , and the spectral quotients  $\beth_1 = 1$ ,  $\beth_2 = 2.982$ . The invariant manifold, the spectral points and a representation of the invariant vector bundle along the periodic orbit can be seen in figure 2.

For ROM identification, the data was generated using 600 trajectories each having 50 points with time step  $\Delta t = 0.8$ . The initial conditions were sampled uniformly from the four dimensional unit ball. The reduced order model is visualised in figure 3. The figures compare our direct calculation from the vector field and the ROM identification (as per section 3.8) from simulation data. The instantaneous frequencies and damping ratios, as calculated by the two methods, are close to each other for lower amplitudes and diverge for higher amplitudes. The relative error of the asymptotic expansion directly from the vector field varies with amplitude, while the data-driven method has a uniform error over the amplitude. This means that the direct calculation can have higher errors at higher amplitudes than the data-driven method. There could

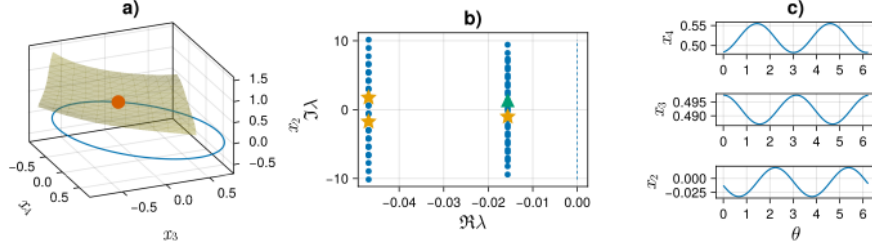


Figure 2: a) The invariant torus and the invariant manifold at one point along the torus. b) The spectrum of the linear dynamics about the torus. The stars denote the representative eigenvalues as selected by (21), the triangle denotes the eigenvalue used for model reduction. c) An incomplete representation of the invariant vector bundle: three out of four coordinates of the first vector that spans the two-dimensional invariant vector bundle.

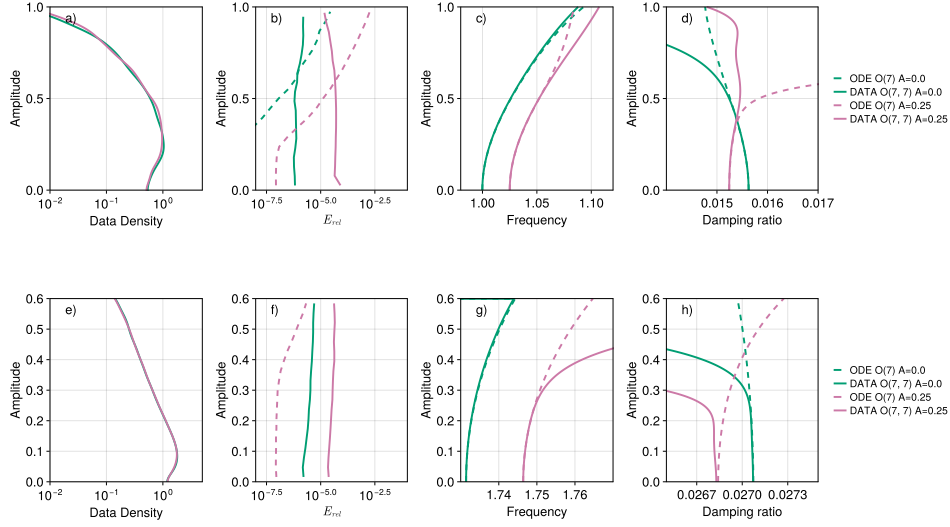


Figure 3: Reduced order models of (47). a,e) The distribution of data along the leaves of the foliation; b,f) the relative error of the invariance equation over the invariant manifold and over the data; c,g) instantaneous frequency of the vibration predicted by the ROM; d,h) instantaneous damping ratio.

be a few reasons for disagreeing calculations at high amplitudes: non-uniqueness of invariant manifolds discussed in the introduction, non-convergence of series expansion (being outside the radius of convergence) or inability to represent the foliation with functions satisfying the constraints (28). The most likely culprit is non-uniqueness, although we have observed through carrying out varying high-order direct calculations that the radius of convergence is only slightly greater than the amplitude where the disagreement of the two calculations occur.

## 4.2 Traffic model on a circular track

We are using a car-following model with a simple optimal velocity function as presented in [21]. The model describes a set of cars running on a circular track. The cars cannot overtake each other and their velocity  $v_k$  is dictated by the distance from the car just in front of them  $h_k$  (called headway). In this particular model drivers reacts instantly to the changes in headway. Each car has a maximum velocity  $V_k$ . The differential equations describing the system are



$$\begin{aligned}\dot{v}_k &= \alpha \left( \frac{V_k (h_k - 1)^2}{1 + (h_k - 1)^2} - v_k \right) & k = 1 \dots n, \\ \dot{h}_k &= v_{k-1} - v_k & k = 2 \dots n, \\ h_1 &= L - \sum_{j=2}^n h_j.\end{aligned}$$

We assume that the length of the circular track is  $L = 2n$ , the maximum velocity of each vehicle is  $V_k = 1$ , except for  $V_n = 1 + A \cos \omega t$ . We set the forcing frequency  $\omega = 0.4374$  and use either  $A = 0$  or  $A = 0.2$  as the forcing amplitude. We also assume  $n = 5$  cars so that semi-analytical calculations are still possible. For this given set of parameters and without forcing, the steady state is such that all headways are equal  $h_k^* = L/n$  and all velocities are

$$v_k^* = \frac{(L/n - 1)^2}{1 + (L/n - 1)^2}.$$

The value  $\alpha = 0.75$  is used so that the system is still stable, but near the stability boundary. The eigenvalues of the Jacobian about this equilibrium are

$$\begin{aligned}\lambda_{12} &= -0.0163 \pm 0.4971i, \\ \lambda_{34} &= -0.2276 \pm 0.7480i, \\ \lambda_{56} &= -0.5223 \pm 0.7480i, \\ \lambda_{78} &= -0.7337 \pm 0.4971i, \\ \lambda_9 &= -0.75.\end{aligned}$$

The spectral quotient for the linear subspace is  $\mathfrak{Q}_{1-2} = 1$  while the spectral quotient for the  $\mathfrak{Q}_{3-9} = 45.993$ . To discretise the system we used  $\ell = 7$  Fourier harmonics and order 7 polynomials. The forced system about the periodic orbit has representative eigenvalues

$$\begin{aligned}\lambda_{12} &= -0.0209 \pm 0.5040i, \\ \lambda_{34} &= -0.2281 \pm 0.7409i, \\ \lambda_{56} &= -0.5203 \pm 0.7409i, \\ \lambda_{78} &= -0.7306 \pm 0.4919i, \\ \lambda_9 &= -0.75.\end{aligned}$$

The spectral quotients are  $\mathfrak{Q}_{1-2} = 1$  and  $\mathfrak{Q}_{3-9} = 33.7454$ . The invariant manifold about a point along the periodic orbit, the spectrum and a representation of the invariant vector bundle can be seen in figure 4. For ROM identification, the data was generated using 600 trajectories each having 50 points with time step  $\Delta t = 0.8$ . The initial conditions were sampled uniformly from the nine-dimensional ball of radius 1.2 about the origin. The ROM associated with the spectrum points  $\lambda_{12}$ , both for the forced and unforced system can be seen in figure 5. As before, the direct calculations and the identified ROMs agree well for lower amplitudes, after which they diverge. The divergence is most likely due to non-uniqueness of invariant manifolds. The levels of error is higher than in the previous example, which can also be attributed to the use of polynomials with compressed tensor coefficients.

## 5 Discussion

We have demonstrated how to identify reduced order models from data using invariant foliations. We have recalled, that if genuine ROMs are sought only invariant foliations can be used. We have discussed how the uniqueness criteria of invariant manifolds and foliations are local to the (quasi-) periodic orbit of the equilibrium and therefore it is impossible to make use of when a ROM is identified from data. This necessitates further work on finding a suitable and data-friendly uniqueness criterion. Despite this issue,

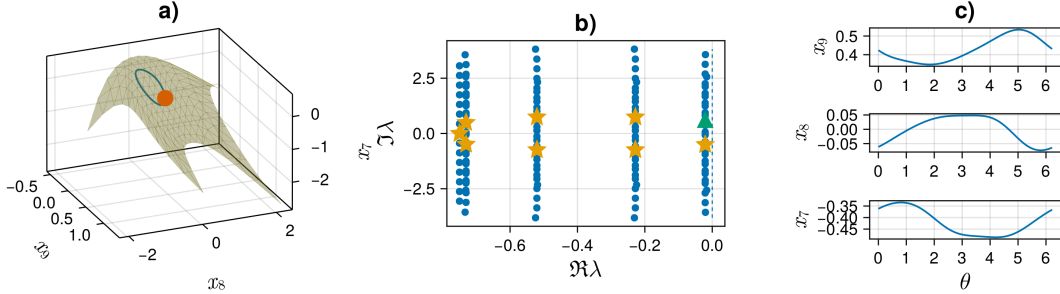


Figure 4: a) The invariant torus and the invariant manifold at one point along the torus. b) The spectrum of the linear dynamics about the torus. The stars denote the representative eigenvalues as selected by (21), the triangle denotes the eigenvalue use for model reduction. c) An incomplete representation of the invariant vector bundle: three out of four coordinates of the first vector that spans the two-dimensional invariant vector bundle.

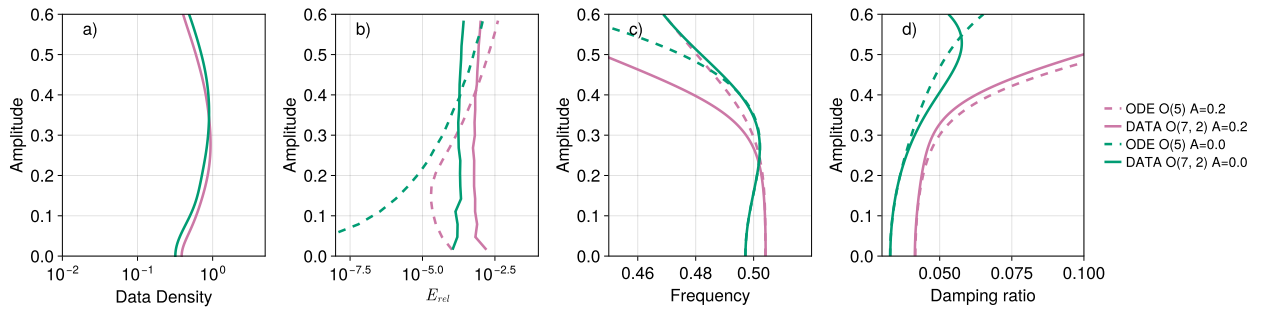


Figure 5: Reduced order models of (47). a) The distribution of data along the leaves of the foliation; b) the relative error of the invariance equation over the invariant manifold and over the data; c) instantaneous frequency of the vibration predicted by the ROM; d) instantaneous damping ratio.

we were able to identify reasonable ROMs at moderate distances from the equilibria and (quasi-) periodic orbits.

In this work we emphasised the use of normal forms for ROM creation as opposed to sparse regression, where the number of model components are singled out using  $L_1$  penalty terms within an optimisation process [6]. Our approach therefore does not require any trade-off between accuracy and model simplicity. The model is always simple, within a suitable coordinate system.

In order to use autoencoders, the data has to lie on a low-dimensional invariant manifold. Running simulations and ignoring the initial transition, as in [9] can be a strategy. This method however has serious flaws. To be able to ignore the initial transient the dynamics of interest must be significantly slower than the rest of the dynamics. However when there is a very slow dynamics, the problem non-uniqueness becomes significant given the large spectral quotient of the invariant manifold. The data can also be skewed and have bias. In fact, autoencoders identify where the data is in the phase space as opposed where the sought after dynamics is.

In the companion paper [28] we have also touched on non-linearisability. In general, the dynamics about an asymptotically stable (quasi-) periodic orbit or equilibrium is linearisable within the basin of attraction. Therefore in [28] a linear ROM within a nonlinear coordinate system could capture nonlinear phenomena remarkably well. However in a data-driven setting, the solution of the invariance equation is not asymptotic but global and approximation errors behave differently. In [27] we have shown that this approximation error causes the data-driven ROM to underestimate the nonlinear dynamics. The present approach of invariant foliations is suitable to capture fully nonlinear dynamics.

**Software** The computer code that produced the results in this paper can be found at <https://github.com/rs1909/Invariant>

## References

- [1] B. Aulbach. The fundamental existence theorem on invariant fiber bundles. *Journal of Difference Equations and Applications*, 3(5-6):267–312, 1998.
- [2] R. H. Bartels and G. W. Stewart. Algorithm 432 [c2]: Solution of the matrix equation  $ax + xb = c$  [f4]. *Commun. ACM*, 15(9):820–826, 1972.
- [3] P. W. Bates, K. Lu, and C. Zeng. Invariant foliations near normally hyperbolic invariant manifolds for semiflows. *Trans. Amer. Math. Soc.*, 352(10):4641–4676, 2000.
- [4] G. Biau and L. Devroye. *Lectures on the Nearest Neighbor Method*. Springer Series in the Data Sciences. Springer, 2015.
- [5] S. Boyd and L. Vandenberghe. *Introduction to Applied Linear Algebra: Vectors, Matrices, and Least Squares*. Cambridge University Press, 2018.
- [6] S.L. Brunton, J.L. Proctor, J.N. Kutz, and W. Bialek. Discovering governing equations from data by sparse identification of nonlinear dynamical systems. *Proceedings of the National Academy of Sciences of the United States of America*, 113(15):3932–3937, 2016.
- [7] X. Cabré, E. Fontich, and R. de la Llave. The parameterization method for invariant manifolds I: Manifolds associated to non-resonant subspaces. *Indiana Univ. Math. J.*, 52:283–328, 2003.
- [8] G. Camps-Valls, A. Gerhardus, U. Ninad, G. Varando, G. Martius, E. Balaguer-Ballester, R. Vinuesa, E. Diaz, L. Zanna, and J. Runge. Discovering causal relations and equations from data. *Physics Reports*, 1044:1–68, 2023.
- [9] M. Cenedese, J. Axås, B. Bäuerlein, K. Avila, and G. Haller. Data-driven modeling and prediction of non-linearizable dynamics via spectral submanifolds. *Nat Commun*, 13(872), 2022.
- [10] K. Champion, B. Lusch, J. Nathan Kutz, and S. L. Brunton. Data-driven discovery of coordinates and governing equations. *Proceedings of the National Academy of Sciences of the United States of America*, 116(45):22445–22451, 2019.

- [11] C. Chicone. *Ordinary Differential Equations with Applications*. Texts in Applied Mathematics. Springer New York, 2008.
- [12] R. de la Llave. Invariant manifolds associated to nonresonant spectral subspaces. *Journal of Statistical Physics*, 87(1):211–249, 1997.
- [13] R. de la Llave and C. E. Wayne. On irwin’s proof of the pseudostable manifold theorem. *Mathematische Zeitschrift*, 219:301–321, 1995.
- [14] J. M. Epstein. Why model? *Journal of Artificial Societies and Social Simulation*, 11(4):12, 2008.
- [15] À. Haro, M. Canadell, Al. Luque, J. M. Mondelo, and J.-L. Figueras. *The Parameterization Method for Invariant Manifolds: From Rigorous Results to Effective Computations*, volume 195 of *Applied Mathematical Sciences*. Springer, 2016.
- [16] M. W. Hirsch, C. C. Pugh, and M. Shub. Invariant manifolds. *Bull. Amer. Math. Soc.*, 76(5):1015–1019, 09 1970.
- [17] I. G. Kevrekidis, C. W. Gear, J. M. Hyman, P. G. Kevrekidis, O. Runborg, and C. Theodoropoulos. Equation-free, coarse-grained multiscale computation: enabling microscopic simulators to perform system-level analysis. *Communications in Mathematical Sciences*, 1(4):715–762, 2003.
- [18] M. A. Kramer. Nonlinear principal component analysis using autoassociative neural networks. *AIChE Journal*, 37(2):233–243, 1991.
- [19] H. Blaine Lawson, Jr. Foliations. *Bull. Amer. Math. Soc.*, 80:369–418, 1974.
- [20] J. Nutini, M. Schmidt, I. H. Laradji, M. Friedlander, and H. Koepke. Coordinate descent converges faster with the gauss-southwell rule than random selection. In *Proceedings of the 32nd International Conference on International Conference on Machine Learning - Volume 37, ICML’15*, pages 1632–1641, 2015.
- [21] G. Orosz, R. E. Wilson, R. Szalai, and G. Stépán. Exciting traffic jams: Nonlinear phenomena behind traffic jam formation on highways. *Phys. Rev. E*, 80:046205, Oct 2009.
- [22] C. Pugh, M. Shub, and A. Wilkinson. Hölder foliations, revisited, 2012.
- [23] A. J. Roberts. Appropriate initial conditions for asymptotic descriptions of the long-term evolution of dynamical systems. *J. Austral. Math. Soc. Ser. B*, 31:48–75, 1989.
- [24] C.E. Shannon. Communication in the presence of noise. *Proceedings of the IRE*, 37(1):10–21, 1949.
- [25] S. W. Shaw and C Pierre. Normal-modes of vibration for nonlinear continuous systems. *J. Sound Vibr.*, 169(3):319–347, 1994.
- [26] R. Szalai. Invariant spectral foliations with applications to model order reduction and synthesis. *Nonlinear Dynamics*, 101(4):2645–2669, 2020.
- [27] R. Szalai. Data-driven reduced order models using invariant foliations, manifolds and autoencoders. *Journal of Nonlinear Science*, 33(5):75, 2023.
- [28] R. Szalai. Non-resonant invariant foliations of quasi-periodically forced systems, 2024.
- [29] L. N. Trefethen. *Spectral Methods in MATLAB*. SIAM Philadelphia, 2000.
- [30] S. Wiggins. *Introduction to Applied Nonlinear Dynamical Systems and Chaos*. Texts in Applied Mathematics. Springer New York, 2003.